ACS APPLIED MATERIALS & INTERFACES

Research Article

www.acsami.org

Polypyrrole-Enveloped Pd and Fe_3O_4 Nanoparticle Binary Hollow and Bowl-Like Superstructures as Recyclable Catalysts for Industrial Wastewater Treatment

Xue Zhang, Min Lin, Xiaoying Lin, Chunting Zhang, Haotong Wei, Hao Zhang,* and Bai Yang

State Key Laboratory of Supramolecular Structure and Materials, College of Chemistry, Jilin University, Changchun 130012, P. R. China

Supporting Information

ABSTRACT: Metal and metal-oxide nanoparticles (NPs) are promising catalysts for dye degradation in wastewater treatment despite the challenges of NP recovery and recycling. In this study, water-dispersible NP superstructures with spherical morphology were constructed from hydrophobic Pd and Fe_3O_4 NPs by virtue of the oil droplets in an oil-in-water microemulsion as templates. Control of the evaporation rate of organic solvents in the oil droplets produces solid, hollow, and bowl-like superstructures. The component Fe_3O_4 and in particular Pd NPs can catalyze H_2O_2 degradation to create hydroxyl radicals and therewith degrade various dyes, and the magnetic Fe_3O_4 NPs also permit recycling of the superstructures with a magnet. Because the hollow and bowl-like superstructures increase the contact area of the NPs with their surroundings in comparison to solid superstructures, the catalytic activity is greatly enhanced. To improve the structural stability, the superstructures were further enveloped with a thin polypyrrole (PPy) shell, which does not weaken the catalytic activity. Because the current method is facile and feasible to create recyclable catalysts, it will promote the practicability of NP catalysts in treating industrial polluted water.

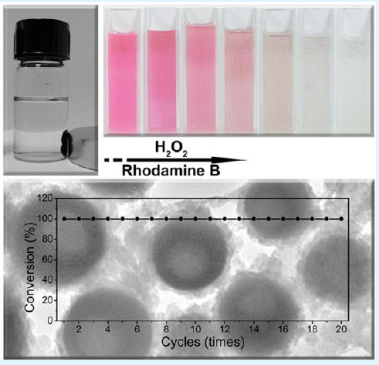

KEYWORDS: *Fe_3O_4 nanoparticles, Pd nanoparticles, superstructure, polypyrrole, wastewater treatment*

INTRODUCTION

Accompanied with the rapid development of modern industry, environmental problems are increasing day by day. Environmental pollution, such as atmospheric, soil, and water pollution, lead to enormous loss both in the economic domain and in human health.[1−4] Among the various forms of pollution, aquatic environment pollution seriously impacts our daily life because water is one of the most important elements to maintain human survival and development. The main cause of water pollution is the discharge of a significant amount of industrial wastewater that has a complex composition of pollutants. For example, the wastewater from the textile industry contains various organic dyes.[5−8] To treat such wastewater, a number of methods for degrading dyes have been tested, such as biodegradation,[9] coagulation,[10] adsorption,[11,12] membrane process,[13] and, in particular, advanced oxidation process (AOP).[14,15] As an efficient method, AOP is based on the creation of reactive species such as hydroxyl radicals ($^{\bullet}OH$) for the destruction of various dyes, which yields CO_2 and inorganic ions without selectivity.[16,17] The typical AOP systems include H_2O_2 plus ultraviolet,[18] H_2O_2 plus Fe^{2+}/Fe^{3+},[19,20] TiO_2-containing materials plus ultraviolet,[21,22] Fe_3O_4 plus H_2O_2,[23,24] Pd-containing materials plus H_2O_2,[25] and so forth. Owing to their high activity, Pd-containing materials are conventionally applied for catalyzing H_2O_2 homolysis, which greatly shortens the duration for dye degradation.[25,26] In addition, these catalysts are conventionally shaped into nanometer-sized units, such as nanoparticles (NPs), because the catalytic activity greatly depends on the increased specific surface area of a given material.[23,24]

Water-dispersibility and recyclability are two major problems for the practical application of nanocatalysts in wastewater treatment.[14,22] Current efforts are attempting to meet the challenge for simultaneously achieving water-dispersibility and recyclability because good water-dispersibility usually results in difficulty separating the nanocatalysts from water. The self-assembly of NP catalysts into higher-order structures, namely, superstructures, is expected to solve this problem[27] because the introduction of other building blocks into the superstructures can bestow diversified functionalities, such as magnetic separation of specific NPs. With respect to self-assembly, many methods have been developed to construct superstructures with controllable size, shape, composition, and surface properties.[28−30] As a tested method to produce water-dispersible NP superstructures, the self-assembly of hydrophobic NPs using the oil droplets in an oil-in-water (O/W) microemulsion as templates yields water-dispersible colloidal microspheres composed of hundreds of NPs.[31,32] Many hydrophobic NPs have been used to construct superstructures with an NP array in an ordered manner, such as Au, Fe_3O_4,

Received: October 13, 2013
Accepted: November 22, 2013
Published: November 22, 2013

CdSe, and $NaYF_4$ NPs, Bi_2S_3 nanoplates, CdSe/CdS nanorods, and so forth.[33−35] Binary superstructures have also been fabricated from two different kinds of NPs, for example, the combination of CdTe and Fe_3O_4, although the NPs lose the ordered array of inner superstructures.[36,37] As an efficient method for functional integration, such a technique is potentially useful for enhancing the performance of nanocatalysts.

The full contact of the component NPs in the superstructures with their external surroundings is also important for enhancing the catalytic efficiency.[28,38] However, for the conventional solid superstructures with diameters around several hundreds nanometers, the inner NPs cannot contact the surroundings, making them useless in catalytic reactions.[27,29] In comparison, hollow or other nonsolid superstructures are expected to increase the contact of NPs with their surroundings despite the complicated process to construct such structures.[39−44]

Herein, we demonstrate the fabrication of Pd/Fe_3O_4 binary hollow and bowl-like superstructures from preformed Pd and Fe_3O_4 NPs on the basis of our previous method for constructing solid superstructures.[45] By simply elevating the evaporation temperature of the organic solvents, the morphologies of the NP superstructures are tuned from solid to hollow to bowl-like spheres. The hollow and bowl-like superstructures present better catalytic activity for catalyzing H_2O_2 homolysis and subsequently promoting dye degradation than solid superstructures. The structural stability is further improved by coating a thin polypyrrole (PPy) shell on the as-prepared superstructures. Catalytic experiments indicate that the PPy shell does not lower the catalytic activity in comparison to bare superstructures.

EXPERIMENTAL SECTION

Materials. Potassium hexachloropalladate (K_2PdCl_6, 99%), iron acetylacetonate ($Fe(acac)_3$, 99.9+%), 1,2-hexadecanediol (90%), benzyl ether (99%), oleyamine (70%), oleic acid (OA, 90%), dodecyltrimethylammonium bromide (DTAB, 99%), and poly(*N*-vinylpyrrolidone) (PVP, $M_w = 5.5 \times 10^4$) were purchased from Sigma-Aldrich. Pyrrole (99%) was purchased from Acros Organics. Gelatin was obtained from Fluka. Sodium borohydride ($NaBH_4$), ethylene glycol, toluene, chloroform, methylene blue (ME), rhodamine B (RhB), neutral red (NR), methyl orange (MO), and $FeCl_3{\cdot}6H_2O$ were analytical grade and used as received. Octadecyl-*p*-vinylbenzyldimethylammonium chloride (OVDAC) was synthesized according to our previous method.[46] Absolute ethanol and deionized water were used in all experiments.

Synthesis of Pd and Fe_3O_4 NPs. OVDAC-stabilized Pd NPs were prepared by reducing K_2PdCl_6 with $NaBH_4$. Ten milliliters of a 15 mM K_2PdCl_6 aqueous solution was mixed with 15 mL of a 7 mg/mL OVDAC chloroform solution. With vigorous stirring, Pd^{4+} was completely transferred from water to chloroform. Then, 4.15 mL of a 9 mg/mL $NaBH_4$ aqueous solution was added dropwise under vigorous stirring. After 30 min of stirring at room temperature, the chloroform phase was separated to achieve OVDAC-stabilized Pd NPs.

OA-stabilized Fe_3O_4 NPs were prepared according to a thermal decomposition method.[47] In 20 mL of phenyl ether, 2 mmol of $Fe(acac)_3$, 10 mmol of 1,2-hexadecanediol, 6 of mmol OA, and 6 mmol of oleylamine were mixed. After stirring for 15 min under a nitrogen atmosphere, the solution was heated at 200 °C, kept at this temperature for 30 min, and then refluxed for another 30 min at 265 °C. After cooling to room temperature, the solution was treated with ethanol. The products were separated with a magnet and redispersed in chloroform to obtain OA-stabilized Fe_3O_4 NPs.

Preparation of Pd, Fe_3O_4, and Pd/Fe_3O_4 Superstructures. DTAB-capped Pd/Fe_3O_4 binary superstructures were prepared by a microemulsion template route according to our previous method.[45] Typically, the experiment started by mixing 5 mg of Pd NPs and 5 mg of Fe_3O_4 NPs in 1 mL of toluene at room temperature. Under mechanical stirring, the NP solution was added dropwise into a DTAB aqueous solution (14 mg/mL, 5 mL) to form an oil-in-water microemulsion. By evaporating toluene at a specific temperatures (e.g., 20, 40, 60, 80, and 100 °C), the DTAB-capped Pd/Fe_3O_4 solid, hollow, and bowl-like superstructures were prepared. The superstructures were collected with a magnet. For comparison, DTAB-capped Pd and Fe_3O_4 unitary superstructures were prepared following a similar method except that Pd and Fe_3O_4 NPs alone were used.

Catalytic Experiments. Four water-soluble organic dyes were chosen to investigate the catalytic activity of Pd/Fe_3O_4 superstructures, which were ME, RhB, NR, and MO. In a typical catalytic experiment, 3 mg of catalyst was mixed with an aqueous solution of RhB (5 mg/L, 10 mL). Under ultrasonic treatment (40 kHz), 1 mL of H_2O_2 was injected into the mixture. The RhB degradation was monitored by UV−vis absorption spectra.

PPy-Enveloped Superstructures. Three milligrams of DTAB-capped Pd, Fe_3O_4, or Pd/Fe_3O_4 superstructures were added into an ethylene glycol solution of PVP (2.0 mM, 5 mL) under mechanical stirring. After 10 min, a gelatin aqueous solution (10 mg/mL, 0.5 mL) was injected into the mixture. The solution was heated at 80 °C for 3 h. After cooling to room temperature, the PVP-capped superstructures were separated from the solution and dispersed in deionized water. Pyrrole monomer was injected into the PVP-capped superstructure solution under mechanical stirring at ambient temperature with specific monomer concentrations of 1.44, 2.88, 8.66, and 14.4 mM. After 0.5 h of stirring, 1 mL of a 10 mg/mL aqueous $FeCl_3{\cdot}6H_2O$ solution was added to initiate the polymerization. With continuous stirring for 12 h, PPy-enveloped superstructures were obtained. Before further characterization, the products were washed with water and ethanol more than three times.

Characterization. Transmission electron microscopy (TEM) was performed using a Hitachi H-800 electron microscope at an acceleration voltage of 200 kV with a CCD camera. High-angle annular dark-field scanning TEM energy-dispersive X-ray spectroscopy (HAADF-STEM-EDS) was conducted with a FEI Tecnai F20 transmission electron microscope at 200 kV. Dynamic light scattering (DLS) measurements were operated with a Zetasizer NanoZS (Malvern Instruments). Inductively coupled plasma (ICP) experiments were performed using a PerkinElmer OPTIMA 3300DV analyzer. UV−vis absorption spectra were measured with a Shimadzu 3600 UV−vis near-IR spectrophotometer. Magnetic measurements were performed using a SQUID magnetometer (QD MPMS) at 300 K by cycling the magnetic field between −10 and 10 kOe. Photoluminescence (PL) spectroscopy was measured using a Shimadzu RF-5301 PC spectrophotometer. The excitation wavelength was 315 nm. Thermogravimetric (TGA) analysis was operated with a Q500 themoanalysis instrument from TA Company. Analyses were carried out under a N_2 flow in the range of 30−900°C with a heating rate of 10.0 °C/min.

RESULTS AND DISCUSSION

In the experiments, OVDAC-stabilized 3.4 nm Pd and OA-stabilized 5.3 nm Fe_3O_4 NPs were employed as the building blocks to fabricate the superstructures (Figure S1). The hydrophobic alkyl chains of OVDAC and OA make the NPs dispersible in common organic solvents, such as toluene. Five milligrams of Pd NPs and 5 mg of Fe_3O_4 NPs were mixed in 1 mL of toluene at room temperature. Under mechanical stirring, the binary NP solution was added dropwise into 5 mL of a 14 mg/mL DTAB aqueous solution to form an O/W microemulsion. After evaporating toluene at 40 °C under stirring, DTAB-capped Pd/Fe_3O_4 binary hollow superstructures were fabricated. Under TEM, the morphology of the superstructures

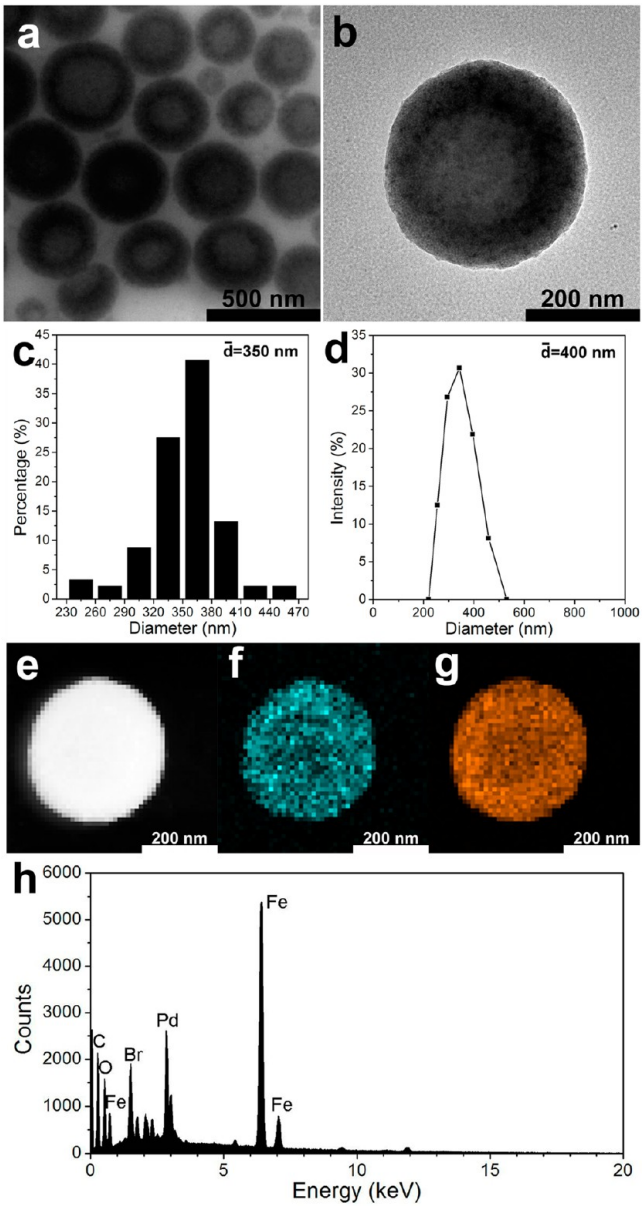

Figure 1. (a, b) TEM images and (c) size distribution of DTAB-capped Pd/Fe_3O_4 binary hollow superstructures. (d) DLS size distribution of the superstructures. (e) HAADF-STEM image of the superstructures and the mapping images of the (f) Pd and (g) Fe elements. (h) EDS spectrum of the superstructures.

appear as hollow spheres with an average diameter of 350 ± 40 nm (Figure 1a–c). DLS measurement indicates an average diameter of 400 nm (Figure 1d), consistent with the TEM result. The EDS spectrum exhibits a homogenous distribution of Pd and Fe elements in the superstructures, confirming that Pd and Fe_3O_4 NPs distribute homogenously rather than form respective aggregates (Figure 1e–g). Meaningfully, the content of the Pd and Fe elements in the middle of the sphere is less than that on the shell, further confirming that the superstructures are hollow spheres (Figure 1f,g). The quantitative analysis of the EDS data reveals a Pd/Fe molar ratio of 1:6.0 (Figure 1h). The Pd/Fe ratio was further confirmed by ICP, which indicates the ratio of 1:8.5.

In general, hollow and bowl-like superstructures were fabricated similarly to our previous works on fabricating solid

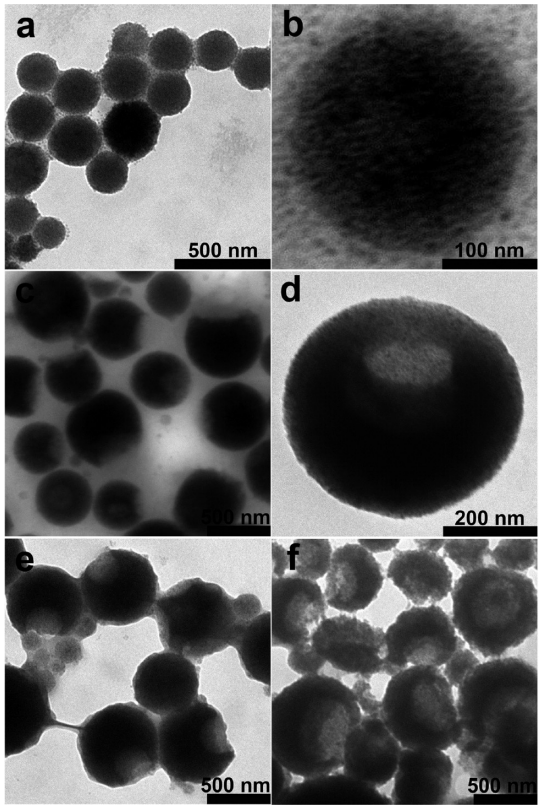

Figure 2. TEM images of DTAB-capped Pd/Fe_3O_4 binary superstructures prepared at (a, b) 20, (c, d) 60, (e) 80, and (f) 100 °C.

superstructures, which employed the oil droplets in an O/W microemulsion as the templates and organic-solvent evaporation to drive the self-assembly of NPs.[36,45] However, the evaporation temperature of the organic solvents was elevated to tune the assembly process (Figure 2). As exhibited by TEM observation, solid superstructures with an average diameter of 220 ± 50 nm were obtained at 20 °C (Figures 2a,b and S2a). Elevating the temperature to 40 °C while fixing the other experimental variables resulted in hollow superstructures with an average diameter of 350 ± 40 nm (Figure 1a–c). Further elevating the temperature to 60 °C generates bowl-like superstructures with an average diameter of 450 ± 80 nm (Figures 2c,d and S2c). These results mean that the temperature simultaneously alters the morphology and increases the diameter of the superstructures. The size increase was also confirmed by DLS measurement (Figures 1d and S2b,d). In addition, the bowl-like structures can be finely controlled by further elevating the evaporation temperature. Occurring simultaneously with a diameter increase of the bowl, the mouth-to-bowl ratio increases as the evaporation temperature is elevated from 60 to 100 °C (Figure 2c–f).

The temperature-dependent morphology variation is understandable according to the interparticle interactions and diffusion rate (V_D) of NPs. In this context, the driving force for NP distribution in oil-droplet template relates to the gravitation of NPs, the van der Waals attraction between NPs, the pressure from surrounding water, and the diffusion effect of NPs caused by solvent evaporation. Only the diffusion effect permits the motion of NPs to the droplet surface, whereas other factors limit NPs in the droplets (Figure 3). In addition, the elevated temperature greatly favors NP diffusion but has less effect on the gravitation, van der Waals attraction, and the

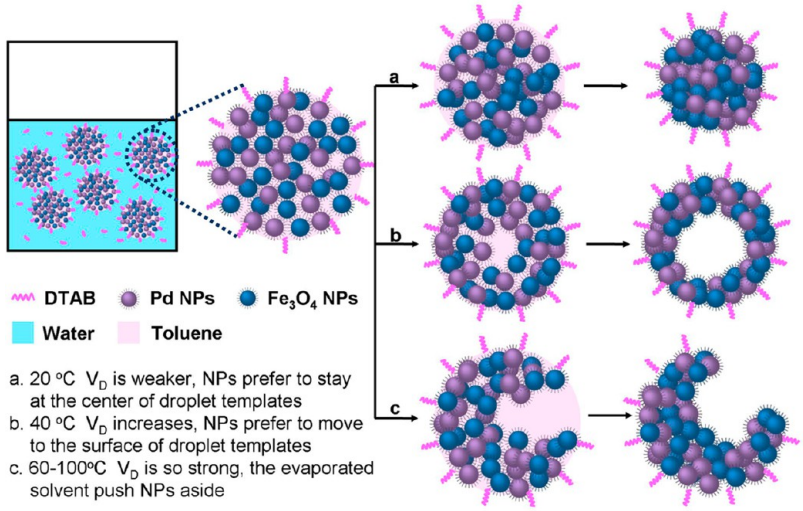

Figure 3. Schematic illustration of the preparative procedure of DTAB-capped Pd/Fe_3O_4 binary superstructures with solid, hollow, and bowl-like morphologies. The fabrication at (a) 20, (b) 40, (c) and 60−100 °C are demonstrated.

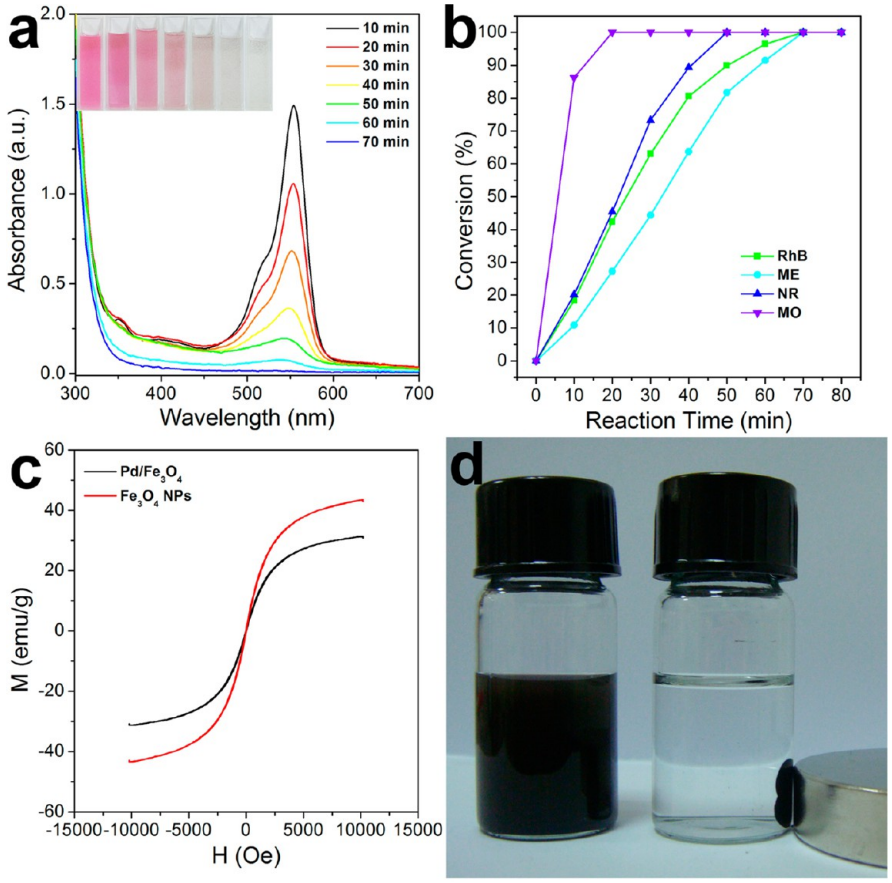

Figure 4. (a) Temporal evolution of the UV−vis absorption spectra of 5 mg/L of a RhB aqueous solution with the addition of 3 mg of Pd/Fe_3O_4 superstructures as the catalyst. The inset shows the corresponding photographs of the solution. (b) Degradation conversion curves of RhB, ME, NR, and MO in the presence of 3 mg of Pd/Fe_3O_4 superstructures. (c) $M(H)$ curves of the superstructures and OA-capped Fe_3O_4 NPs. (d) Photograph of DTAB-capped Pd/Fe_3O_4 superstructure suspension without and with a magnet.

pressure from surrounding water. As a result, at relatively low evaporation temperatures, NPs prefer to stay at the center of the droplet templates because the diffusion effect is weaker than the sum of the other factors. This produces solid superstructures after solvent evaporation (Figure 2a). In contrast, V_D increases with the increment of temperature, favoring the motion of NPs toward the droplet surface and increasing the possibility of forming hollow structures (Figure 1a). As the temperature is further increased, the rapid solvent evaporation pushes the NPs aside, thus producing bowl-like superstructures (Figure 2c−f). The extremely fast solvent evaporation at 100 °C seriously destroys the hollow structures and subsequently

dx.doi.org/10.1021/am404440d | ACS Appl. Mater. Interfaces 2014, 6, 450−458

Table 1. Comparison of the Degradation Time of RhB, ME, NR, and MO with the Addition of 3 mg of DTAB-Capped Pd/Fe_3O_4 Solid Superstructures and DTAB-Capped Solid, Hollow, and Bowl-Like Pd/Fe_3O_4 Superstructures as the Catalysts[a]

	degradation time (min)			
catalysts	RhB	ME	NR	MO
hollow Pd/Fe_3O_4	70	70	50	20
bowl Pd/Fe_3O_4	50	70	50	20
solid Pd/Fe_3O_4	100	100	70	40
solid Pd	40	50	30	20
solid Fe_3O_4	160	130	70	50

[a]The degradation time was confirmed according to the absorption spectra.

produces the bowl-like superstructures with a high mouth-to-bowl ratio (Figure 2f).

Four common organic dyes in industrial wastewater, ME, RhB, NR, and MO, were chosen to investigate the catalytic activity of the Pd/Fe_3O_4 binary hollow superstructures. In a typical catalytic experiment, 3 mg of catalyst are mixed with a 10 mL aqueous solution of 5 mg/L RhB. Under ultrasonic treatment (40 kHz), 1 mL of H_2O_2 is injected into the mixture. RhB degradation is monitored by the UV−vis absorption spectra (Figure 4a). With prolonging the duration of these conditions, the absorption of RhB at 550 nm gradually decreases and completely disappears after 70 min. Meanwhile, the color of the solution turns from pink to colorless (Figure 4a, inset). These data prove the high catalytic activity of the superstructures in promoting RhB degradation. Besides RhB, the Pd/Fe_3O_4 superstructures are also efficient in catalyzing ME, NR, and MO degradation (Figure S3). ME, NR, and MO completely degrade within 70, 50, and 20 min, respectively (Figure 4b). The different degradation rates of the four dyes is mainly attributed to their charges. In the current system, dye degradation is based on an advanced oxidation process using $^{\bullet}OH$ to destroy the molecular structures. The $^{\bullet}OH$ is generated on the surface of nanocatalysts, so the interactions between catalysts and dyes greatly influence the catalytic efficiency. As shown in Table 1, the catalysts are capped by DTAB, a positive surfactant, which bestows the catalysts with positive charges. Although RhB and ME possess positive charge, NR is near neutral, and MO possesses negative charge (Figure S4). The electrostatic repulsion−attraction between catalysts and dyes leads to the increasing degradation rate following the sequence of RhB, ME, NR, and MO. In addition, the chemical structures of RhB, ME, and NR are more complex than MO, which also increases the steric hindrance and complexity of the reaction with $^{\bullet}OH$. As a result, RhB and ME exhibit the slowest degradation rate, then NR, and finally MO. Note that the dyes do not degrade in the absence of the superstructures (Figure S5) because the homolysis of H_2O_2 to $^{\bullet}OH$ is not facilitated. Instead, the heterolysis to H_2O and O_2 is favored.

The magnetic curves of Fe_3O_4 NPs and Pd/Fe_3O_4 superstructures were compared by cycling the magnetic field

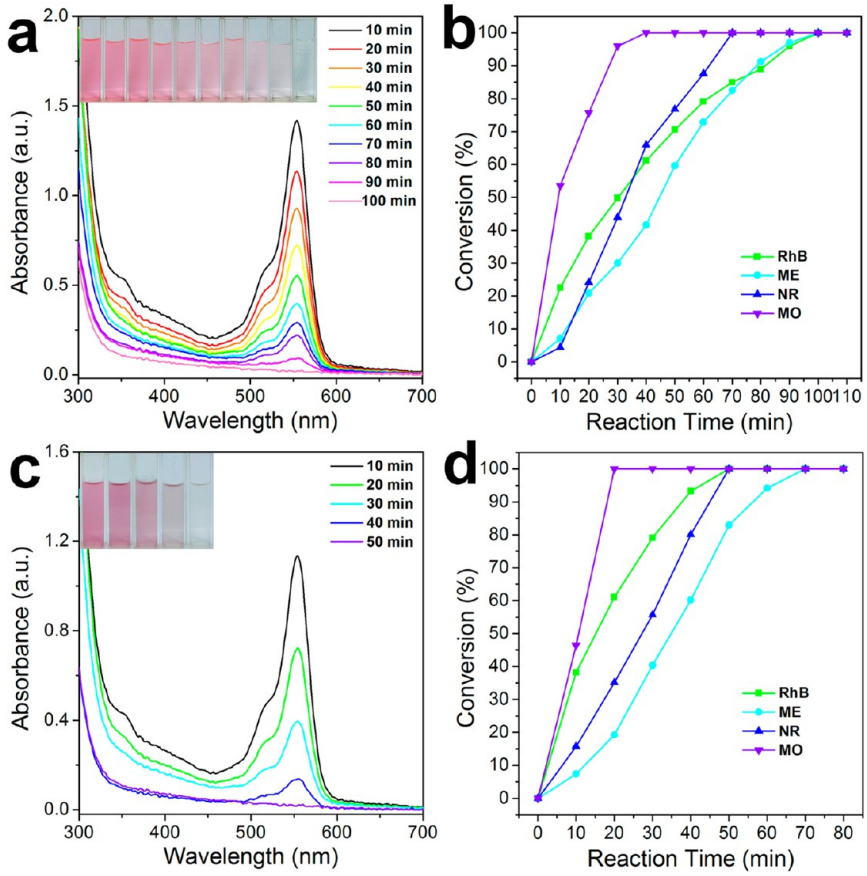

Figure 5. Temporal evolution of the UV−vis absorption spectra of a 5 mg/L RhB aqueous solution with the addition of 3 mg of Pd/Fe_3O_4 (a) solid and (c) bowl-like superstructures as the catalysts. The inset shows the corresponding photographs of the solution. Degradation conversion curves of RhB, ME, NR, and MO in the presence of 3 mg of Pd/Fe_3O_4 (b) solid and (d) bowl-like superstructures.

dx.doi.org/10.1021/am404440d | ACS Appl. Mater. Interfaces 2014, 6, 450−458

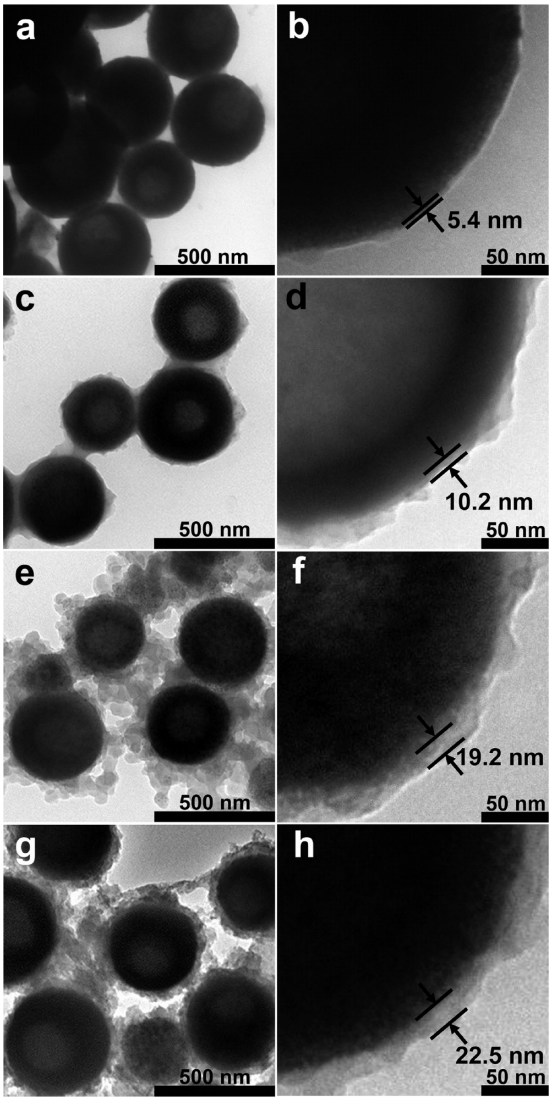

Figure 6. TEM images of PPy-enveloped Pd/Fe_3O_4 superstructures that were prepared with the addition of (a) 1.44, (c) 2.88, (e) 8.66, and (g) 14.4 mM pyrrole. (b, d, f, and h) Corresponding enlarged images to show the thickness of the PPy shell.

between −10 and 10 Oe (Figure 4c). The saturation magnetization of Fe_3O_4 NPs and Pd/Fe_3O_4 superstructures is 43 and 30 emu/g, respectively. The $M(H)$ hysteresis curves are completely reversible, indicating that both the NPs and superstructures are superparamagnetic. The decrease in the saturation magnetization of the superstructures is attributed to the introduction of Pd NPs and hence the decrease of the Fe_3O_4 component. Despite the lowered magnetism, the superstructures can be separated from the catalytic systems with the help of a magnet (Figure 4d). This will facilitate the recycling of the nanocatalysts in wastewater treatment.

Because the activity of nanocatalysts relates to the contact area with dyes, the catalytic efficiency of the superstructures may depend on the morphology. Hollow and bowl-like superstructures are expected to present better catalytic activity than solid ones. To confirm this, the catalytic activity of solid, hollow, and bowl-like superstructures with the same diameter and quality were compared for the degradation of ME, RhB, NR, and MO (Figures 4a,b, 5, and S6). As shown in Figure 5a, the degradation time of RhB in the presence of solid superstructures is longer than that of hollow superstructures. The same tendency is also observed for the degradation of ME, NR, and MO (Figure 5b). The degradation time of dyes in the presence of bowl-like superstructures is similar to that for hollow ones (Figure 5c,d). Figure S7 shows the corresponding temporal evolution of the UV−vis absorption spectra of ME, NR, and MO using solid and bowl-like superstructures as catalysts. The degradation time of the four dyes in the presence of different superstructures is displayed in Table 1. Hollow and bowl-like superstructures present better catalytic activity than solid superstructures because of their high contact area with the dyes.

For a comparison, Pd NP superstructures and Fe_3O_4 NP superstructures were also fabricated and used to test the catalytic activity (Figure S8). As shown in Table 1, both Pd and Fe_3O_4 superstructures are capable of catalyzing dye degradation. However, Pd superstructures possess higher activity than that of Fe_3O_4, represented by the shorter duration for complete degradation. The activity of Pd/Fe_3O_4 binary superstructures is slightly lower than Pd superstructures, which is attributed to the presence of Fe_3O_4 in the superstructures. Terephthalic acid was chosen as the detector to test the generation of $^{\bullet}OH$ from H_2O_2 homolysis (Figure S9) because terephthalic acid can trap $^{\bullet}OH$ and create fluorescent 2-hydroxyterephthalic acid.[24] The PL spectra indicate that the emission intensity of terephthalic acid solution decreases following the sequence of Pd, Pd/Fe_3O_4, and Fe_3O_4 superstructures, confirming the generation of more $^{\bullet}OH$ and subsequent 2-hydroxyterephthalic acid by Pd catalysis.

The catalytic activity and stability of directly dispersed NPs was also studied by transferring hydrophobic Pd and Fe_3O_4 NPs to water rather than forming superstructures (Figure S10a,b). As shown in Figure S10c,d, RhB degrades within 30 and 60 min, respectively, using directly dispersed Pd and Fe_3O_4 NPs as catalysts, which presents higher catalytic activity than the superstructures. This is mainly attributed to the high specific surface area of the directly dispersed NPs, consistent with the previous discussions. However, serious aggregation of directly dispersed NPs was observed after only one use in the catalytic reaction because of their poor stability (Figure S10e,f). In contrast, the superstructures demonstrate an improved structural stability and magnetic separation property, although their stability is still not that good.

As mentioned, although Pd/Fe_3O_4 binary superstructures exhibit potential for use in applications in catalyzing dye degradation and catalyst recycling, the structural stability of the superstructures is still poor. The structures are easy to deconstruct under ultrasonication, organic solvents, or even during storage. This is attributed to the weak interparticle interactions between the neighboring NPs within the superstructures.[34] Pd and Fe_3O_4 NPs are capped by hydrophobic alkyl ligands. van der Waals interactions are the main driving force to maintain the structures. In comparison to covalent linkage, van der Waals interactions are much weaker. This feature undoubtedly limits their practical applications. To improve the structural stability, a PPy shell was coated outside the superstructures via oxidative polymerization. TEM observation confirmed that the superstructures were well-maintained after the catalytic reaction (Figure S11c). In comparison, both DTAB- and PVP-capped superstructures deconstruct and finally aggregate (Figure S11a,b). By altering the concentration of pyrrole monomer, the thickness of the PPy shell is also tunable. As shown in Figure 6, PPy thicknesses of

dx.doi.org/10.1021/am404440d | ACS Appl. Mater. Interfaces 2014, 6, 450−458

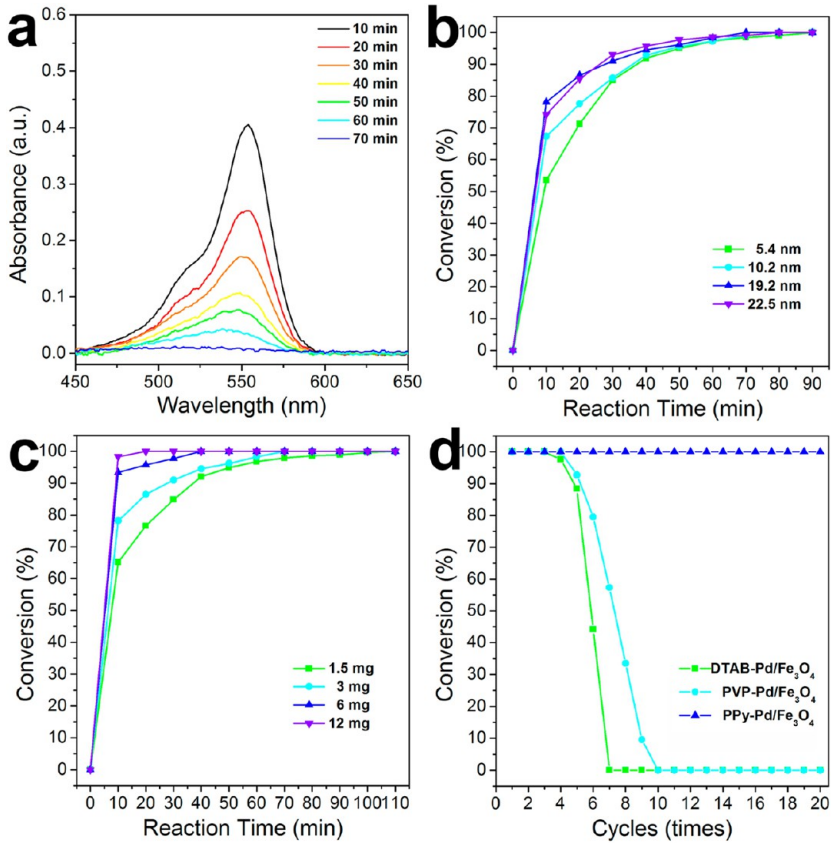

Figure 7. (a) Temporal evolution of the UV−vis absorption spectra of an RhB aqueous solution in the presence of 5 mg of PPy-enveloped Pd/Fe_3O_4 superstructures. (b) Effect of PPy thickness on the degradation of RhB. The thickness of the PPy shell is 5.4, 10.2, 19.2, and 22.5 nm, respectively. (c) Effect of superstructure dosage on the degradation rate of RhB. (d) Comparison of the structural stability of DTAB-, PVP-, and PPy-capped superstructures over the course of 20 cycles of reuse for catalyzing RhB degradation.

5.4, 10.2, 19.2, and 22.5 nm were achieved through the addition of 1.44, 2.88, 8.66, and 14.4 mM pyrrole, respectively. TGA analysis was further employed to characterize the PPy shell (Figure S12). After formation of the PPy shell, the organic content greatly increases in comparison to the PPy-free superstructures. Control experiments further revealed that with increasing pyrrole monomer the organic content also increases, implying the growth of the PPy shell. By comparing then with PPy-free superstructures, the weight ratio of the PPy shell was calculated to be 7.3, 12.6, 15.1, and 21.0% for the four pyrrole feed amounts, respectively. The corresponding thickness of the PPy shell was further estimated to be 7.8, 12.2, 17.3, and 25.5 nm, basically consistent with the TEM observation (Figure 6).

RhB was chosen to reveal the influence of the PPy shell on the catalytic activity of superstructures. As shown in Figure 7a, RhB absorption gradually decreases and completely disappears within 70 min. In comparison to DTAB-capped superstructures, the catalytic activity of PPy-enveloped ones does not change obviously (Figures 4a and 7a). Except at the initial stage, the PPy shell thickness has no effect on the absorbance variation within the range of 5.4 to 22.5 nm (Figure 7b). This is attributed to the porous structure of the PPy shell, which permits the permeation of small molecules but inhibits nanometer-sized particles and clusters.[48] The rapid decrease of RhB absorbance at the initial stage is attributed to the dye adsorption on PPy, thus promoting the contact of the dyes with the catalysts. To prove this, the temporal evolution of the UV−vis absorption spectra of the mixture of pure PPy particles and RhB were studied (Figure S13a). Except at the beginning, no obvious absorbance decrease occurs during the prolonged reaction, confirming that PPy has no catalytic activity for H_2O_2 homolysis. Similar results were obtained for the degradation of ME, NR, and MO (Figure S13b). In addition, the same effect was observed for PPy-capped bowl-like superstructures as catalysts (Figure S13c,d).

To reveal the concentration effect of the superstructures on RhB degradation, 1.5, 3, 6, and 12 mg of PPy-enveloped superstructures were added into the catalytic system. The degradation conversion curves indicate that the degradation time of RhB is greatly shortened by increasing the dose of superstructures (Figure 7c). With the addition of 12 mg of superstructures, RhB fully degrades within 20 min. Because of the excellent catalytic activity of Pd NPs, the magnetism of Fe_3O_4 NPs, and the structural stability by PPy envelopment, the PPy-enveloped Pd/Fe_3O_4 superstructures present the capability of recycled use for catalyzing dye degradation. A 20 time recycling catalytic experiment was carried out using DTAB-, PVP-, and PPy-capped superstructures as the catalysts (Figure 7d). PPy-capped superstructures maintain excellent catalytic activity after 20 cycles, whereas DTAB- and PVP-capped ones gradually lose the activity after 7 and 10 cycles, respectively. These results confirm that PPy envelopment greatly prevents the deconstruction of the superstructures and therewith improves the recyclability of the nanocatalysts.

CONCLUSIONS

Hydrophobic Pd and Fe_3O_4 NPs were employed as the building blocks for constructing binary hollow and bowl-like superstructures by virtue of oil droplets in an O/W microemulsion as the templates. In comparison to solid superstructures, the hollow and bowl-like superstructures present improved activities in catalyzing dye degradation. A PPy shell was further coated on the as-prepared superstructures via oxidative polymerization. By combining the high catalytic activity of Pd NPs, the magnetism of the Fe_3O_4 NPs, and the protection from the PPy shell, the PPy-enveloped Pd/Fe_3O_4 superstructures act as recyclable catalysts to promote dye degradation. Catalytic tests also confirmed that a thin PPy shell does not weaken catalytic activity. As efficient nanocatalysts, PPy-enveloped Pd/Fe_3O_4 superstructures are potentially applicable in the treatment of industrial wastewater.

ASSOCIATED CONTENT

Supporting Information

TEM images of Pd and Fe_3O_4 NPs, various Pd/Fe_3O_4 binary superstructures, and the superstructures after catalytic reaction; size distribution of Pd/Fe_3O_4 superstructures; catalytic experiments of RhB, ME, NR, and MO degradation in the presence and absence of Pd/Fe_3O_4 superstructures; catalytic experiments of directly dispersed Pd and Fe_3O_4 NPs and pure PPy particles; TGA analysis of PPy-enveloped superstructures; and detection of produced $^{\bullet}OH$. This material is available free of charge via the Internet at http://pubs.acs.org.

AUTHOR INFORMATION

Corresponding Author

*Fax: +86 431 85193423; Tel.: +86 431 85159205; E-mail: hao_zhang@jlu.edu.cn.

Notes

The authors declare no competing financial interest.

ACKNOWLEDGMENTS

This work was supported by the 973 Program of China (2014CB643503), the NSFC (21374042, 21174051, and 21221063), the Natural Science Foundation of Jilin Province (201215030), and the Special Project from MOST of China.

REFERENCES

(1) Jacobson, M. Z. *Energy Environ. Sci.* **2009**, *2*, 148−173.
(2) Sun, J.; Bertos, M. F.; Simons, S. J. R. *Energy Environ. Sci.* **2008**, *1*, 370−377.
(3) Demoling, L. A.; Baath, E. *Environ. Sci. Technol.* **2008**, *42*, 6917−6921.
(4) He, H. B.; Li, B.; Dong, J. P.; Lei, Y. Y.; Wang, T. L.; Yu, Q. W.; Feng, Y. Q.; Sun, Y. B. *ACS Appl. Mater. Interfaces* **2013**, *5*, 8058−8066.
(5) Wang, Y. J.; Chen, J. P.; Lu, L. L.; Lin, Z. *ACS Appl. Mater. Interfaces* **2013**, *5*, 7698−7703.
(6) Lindstrom, A. B.; Strynar, M. J.; Delinsky, A. D.; Nakayama, S. F.; McMillan, L.; Libelo, E. L.; Neill, M.; Thomas, L. *Environ. Sci. Technol.* **2011**, *45*, 8015−8021.
(7) Xiao, S. L.; Wu, S. Q.; Shen, M. W.; Guo, R.; Huang, Q. G.; Wang, S. Y.; Shi, X. Y. *ACS Appl. Mater. Interfaces* **2009**, *1*, 2848−2855.
(8) Wang, J. Q.; Liu, Y. H.; Chen, M. W.; Xie, G. Q.; Louzguine-Luzgin, D. V.; Inoue, A.; Perepezko, J. H. *Adv. Funct. Mater.* **2012**, *22*, 2567−2570.
(9) Sekar, S.; Surianarayanan, M.; Ranganathan, V.; MacFarlane, D. R.; Mandal, A. B. *Environ. Sci. Technol.* **2012**, *46*, 4902−4908.
(10) Canizares, P.; Martinez, F.; Jimenez, C.; Lobato, J.; Rodrigo, M. A. *Environ. Sci. Technol.* **2006**, *40*, 6418−6424.
(11) Zhou, L.; He, B. Z.; Huang, J. C. *ACS Appl. Mater. Interfaces* **2013**, *5*, 8678−8685.
(12) Zhuang, X.; Wan, Y.; Feng, C. M.; Shen, Y.; Zhao, D. Y. *Chem. Mater.* **2009**, *21*, 706−716.
(13) Laera, G.; Cassano, D.; Lopez, A.; Pinto, A.; Pollice, A.; Ricco, G.; Mascolo, G. *Environ. Sci. Technol.* **2012**, *46*, 1010−1018.
(14) Priya, D. N.; Modak, J. M.; Raichur, A. M. *ACS Appl. Mater. Interfaces* **2009**, *1*, 2684−2693.
(15) Oller, I.; Malato, S.; Sanchez-Perez, J. A. *Sci. Total Environ.* **2011**, *409*, 4141−4166.
(16) Chan, S. H. S.; Wu, T. Y.; Juan, J. C.; Teh, C. Y. *J. Chem. Technol. Biotechnol.* **2011**, *86*, 1130−1158.
(17) Wojnarovits, L.; Takacs, E. *Radiat. Phys. Chem.* **2008**, *77*, 225−244.
(18) Keen, O. S.; Baik, S.; Linden, K. G.; Aga, D. S.; Love, N. G. *Environ. Sci. Technol.* **2012**, *46*, 6222−6227.
(19) Spadaro, J. T.; Isabelle, L.; Renganathan, V. *Environ. Sci. Technol.* **1994**, *28*, 1389−1393.
(20) Ma, J. H.; Ma, W. H.; Song, W. J.; Chen, C. C.; Tang, Y. L.; Zhao, J. C. *Environ. Sci. Technol.* **2006**, *40*, 618−624.
(21) Nakata, K.; Kagawa, T.; Sakai, M.; Liu, S. H.; Ochiai, T.; Sakai, H.; Murakami, T.; Abe, M.; Fujishima, A. *ACS Appl. Mater. Interfaces* **2013**, *5*, 500−504.
(22) Yao, W. F.; Zhang, B.; Huang, C. P.; Ma, C.; Song, X. L.; Xu, Q. J. *J. Mater. Chem.* **2012**, *22*, 4050−4055.
(23) Xing, S. T.; Zhou, Z. C.; Ma, Z. C.; Wu, Y. S. *Appl. Catal., B* **2011**, *107*, 386−392.
(24) Wang, N.; Zhu, L. H.; Wang, M. Q.; Wang, D. L.; Tang, H. Q. *Ultrason. Sonochem.* **2010**, *17*, 78−83.
(25) Yuan, S. H.; Fan, Y.; Zhang, Y. C.; Tong, M.; Liao, P. *Environ. Sci. Technol.* **2011**, *45*, 8514−8520.
(26) Choudhary, V. R.; Samanta, C.; Jana, P. *Appl. Catal., A* **2007**, *332*, 70−78.
(27) Colfen, H.; Antonietti, M. *Angew. Chem., Int. Ed.* **2005**, *44*, 5576−5591.
(28) Song, C. Y.; Wang, Y.; Rosi, N. L. *Angew. Chem., Int. Ed.* **2013**, *52*, 3993−3995.
(29) Singh, A.; Coughlan, C.; Laffir, F.; Ryan, K. M. *ACS Nano* **2012**, *6*, 6977−6983.
(30) Riehle, F. S.; Bienert, R.; Thomann, R.; Urban, G. A.; Kruger, M. *Nano Lett.* **2009**, *9*, 514−518.
(31) Wang, T.; LaMontagne, D.; Lynch, J.; Zhuang, J. Q.; Cao, Y. C. *Chem. Soc. Rev.* **2013**, *42*, 2804−2823.
(32) Zhang, H.; Liu, Y.; Yao, D.; Yang, B. *Chem. Soc. Rev.* **2012**, *41*, 6066−6088.
(33) Wang, T.; Zhuang, J. Q.; Lynch, J.; Chen, O.; Wang, Z. L.; Wang, X. R.; LaMontagne, D.; Wu, H. M.; Wang, Z. W.; Cao, Y. C. *Science* **2012**, *338*, 358−363.
(34) Zhuang, J. Q.; Wu, H. M.; Yang, Y. A.; Cao, Y. C. *Angew. Chem., Int. Ed.* **2008**, *47*, 2208−2212.
(35) Bai, F.; Wang, D. S.; Huo, Z. Y.; Chen, W.; Liu, L. P.; Liang, X.; Chen, C.; Wang, X.; Peng, Q.; Li, Y. D. *Angew. Chem., Int. Ed.* **2007**, *46*, 6650−6653.
(36) Han, J. S.; Zhang, X.; Zhou, Y. B.; Ning, Y.; Wu, J.; Liang, S.; Sun, H. Z.; Zhang, H.; Yang, B. *J. Mater. Chem.* **2012**, *22*, 2679−2686.
(37) Li, P.; Peng, Q.; Li, Y. D. *Adv. Mater.* **2009**, *21*, 1945−1948.
(38) Wang, X.; Liao, M. Y.; Zhong, Y. T.; Zheng, J. Y.; Tian, W.; Zhai, T. Y.; Zhi, C. Y.; Ma, Y.; Yao, J. N.; Bando, Y.; Golberg, D. *Adv. Mater.* **2012**, *24*, 3421−3425.
(39) Lou, X. W.; Archer, L. A.; Yang, Z. C. *Adv. Mater.* **2008**, *20*, 3987−4019.
(40) Yu, L.; Wu, H. B.; Lou, X. W. *Adv. Mater.* **2013**, *25*, 2296−2300.
(41) Wu, H. X.; Zhang, S. J.; Zhang, J. M.; Liu, G.; Shi, J. L.; Zhang, L. X.; Cui, X. Z.; Ruan, M. L.; He, Q. J.; Bu, W. B. *Adv. Funct. Mater.* **2011**, *21*, 1850−1862.
(42) Fan, W.; Zhang, C.; Tjiu, W. W.; Pramoda, K. P.; He, C. B.; Liu, T. X. *ACS Appl. Mater. Interfaces* **2013**, *5*, 3382−3391.

(43) Hu, J.; Chen, M.; Fang, X. S.; Wu, L. M. *Chem. Soc. Rev.* **2011**, *40*, 5472−5491.
(44) He, J.; Liu, Y. J.; Babu, T.; Wei, Z. J.; Nie, Z. H. *J. Am. Chem. Soc.* **2012**, *134*, 11342−11345.
(45) Zhang, X.; Han, J. S.; Yao, T. J.; Wu, J.; Zhang, H.; Zhang, H.; Zhang, X. D.; Yang, B. *CrystEngComm* **2011**, *13*, 5674−5676.
(46) Zhang, H.; Wang, C. L.; Li, M. J.; Ji, X. L.; Zhang, J. H.; Yang, B. *Chem. Mater.* **2005**, *17*, 4783−4788.
(47) Sun, S. H.; Zeng, H. *J. Am. Chem. Soc.* **2002**, *124*, 8204−8205.
(48) Hao, L.; Zhu, C.; Chen, C.; Kang, P.; Hu, Y.; Fan, W.; Chen, Z. *Synth. Met.* **2003**, *139*, 391−396.